

DOI: 10.1070/QEL16171

Influence of the input radiation pulse characteristics on the parameters of a XeF(C–A) amplifier in a THL-100 laser system

A.G. Yastremskii, N.G. Ivanov, V.F. Losev

Abstract. **We report the results of experimental and theoretical investigations on the influence of spatial and energy parameters of input radiation with a pulse duration of 50 ps on output characteristics of a XeF(C–A) amplifier in a visible-range, multi-terawatt THL-100 laser system. Dynamics of the energy density radial distribution for laser radiation passing through the amplifier is studied. Results of numerical simulation are presented for amplification of laser beams with Gaussian and super-Gaussian radial energy density distributions. It is shown that the laser energy of 3.2 J obtained experimentally is not the limiting value. According to calculations, the output energy of the amplifier with such mirror configuration may reach 4.1 J, which in the case of a pulse compressed down to 50 fs corresponds to the radiation power of 82 TW.**

Keywords: *THL-100 hybrid laser system, radial intensity distribution, maximal laser radiation energy, numerical simulation.*

1. Introduction

In the late 1970s, laser oscillation was obtained on the transitions B(1/2) → X(1/2) and C(3/2) → A(3/2) of the XeF molecule in photo-dissociation of XeF_2 molecules under vacuum UV (VUV) irradiation [1, 2]. Then, Mikheev et al. (Lebedev Physics Institute) [3–7] showed a promising employment of the transition C(3/2) → A(3/2) of the XeF molecule for direct amplification of femtosecond laser pulses, and a hybrid scheme for multi-terawatt laser systems was suggested.

Using this scheme, at the Institute of High Current Electronics, SB RAS and P.N. Lebedev Physics Institute a hybrid THL-100 laser system was fabricated, which comprised a Ti:sapphire front-end unit, second harmonic oscillator, stretcher on a prism pair, photochemical XeF(C–A) amplifier and compressor on fused silica plates [8, 9]. First experimental investigations carried out with this system yielded a record high laser radiation power of 14 TW in the visible spectral range (λ = 475 nm) at a 50-fs pulse duration [8, 9]. Numerical simulation of picosecond pulse amplification in the active medium of the XeF(C–A) amplifier for various medium compositions and characteristics of the input pulse has shown that kinetics of processes in this system has a potential to increase the laser pulse energy to 3 J and higher [10, 11].

Improvement of the THL-100 laser system in 2015 increased the output power of the XeF(C–A) amplifier to 2 J for a 2-ps, 0.8-mJ pulse [12]. However, the radiation intensity distribution at the amplifier input was not homogenous enough. In the result, due to Kerr nonlinearilty, radiation small-scale self-focusing arose, which resulted in defects on mirror surfaces. A numerical study of amplification in this regime has shown that the maximal intensity of laser radiation reaches 64 GW cm^{-2} [12]. To avoid the small-scale self-focusing of the amplified beam, the input pulse duration was increased to 50 ps (a positively chirped pulse), which allowed one to obtain a Gaussian beam and provided a substantially lower maximal intensity of laser radiation in the XeF(C–A) amplifier [13]. It was not clear in what way these changes would affect the amplification regime.

The aim of this work is to study the influence of the energy value and spatial intensity distribution of input 50-ps pulsed radiation on output parameters of the XeF(C–A) amplifier and investigate conditions for obtaining a limiting high value of radiation energy.

2. Experimental setup and methods

A master oscillator of the front-end complex formed 50-fs transform-limited radiation pulses at a centre wavelength of 950 nm that were then expanded to a FWHM duration of ~100 ps in a stretcher and amplified in Ti:sapphire amplifiers to an energy of 57 mJ. Conversion to the second harmonic occurred in a 2-mm-thick KDP crystal. The second harmonic beam with a Gaussian intensity distribution had a diameter of 3.5 mm (with respect to the 1/e^2 level); the pulse duration and energy were 50 ps and 7 mJ, respectively. Then, the beam was expanded in a mirror telescope with magnification 3$^\times$ and amplified in the multipass optical system of the XeF(C–A) amplifier comprised of 32 mirrors.

In order to avoid diffraction on the mirrors of the XeF(C–A) amplifier, the input radiation passed through a tooth-like diaphragm with the inner diameter of 11 mm and the height-to-step tooth ratio h/d = 7. The beam expanded during amplification and at the 31st transit its radius reached 30 mm. At the last two passes the beam radius increased to 60 mm because the output mirror was convex.

The gas mixture of the XeF(C–A) amplifier consisted of a buffer nitrogen gas (380 Torr) and XeF_2 vapours (0.2 Torr). The active medium [$XeF(C_0)$ molecules] was produced in dissociation of XeF_2 molecules by VUV pump radiation having a wavelength of 172 nm [7, 8]. The energy of laser radiation was measured with Gentec and OPHIR instruments.

A.G. Yastremskii, N.G. Ivanov Institute of High Current Electronics, Siberian Branch, Russian Academy of Sciences, Akademicheskii prosp. 2/3, 634055 Tomsk, Russia; e-mail: yastrems@lgl.hcei.tsc.ru; **V.F. Losev** Institute of High Current Electronics, Siberian Branch, Russian Academy of Sciences, Akademicheskii prosp. 2/3, 634055 Tomsk, Russia; Tomsk Polytechnic University, prosp. Lenina 30, 634050 Tomsk, Russia

Received 5 July 2016; revision received 29 September 2016
Kvantovaya Elektronika **46** (11) 982–988 (2016)
Translated by N.A. Raspopov

3. Numerical model of the amplifier

A scheme of the input unit of the XeF(C–A) amplifier is shown in Fig. 1, where mirror positions (and their relative dimensions) are shown. In the cross section, the laser chamber has a shape of regular hexagon. Its sides are windows through which the pump VUV radiation is launched. The mirror number corresponds to the number of the beam transit in the active volume that closes at this mirror. A similar mirror block is placed at the output end of the amplifier. Mirrors of the input block have even numbers and the numbers of mirrors in the output block are odd. The input beam is introduced into the amplifier through window 0, passes through the amplifier and reflects from mirror 1 placed on the output block of the amplifier. Then, having passed again through the amplifier, the beam reflects from mirror 2 and so on. After the 33th round over the active medium, the laser beam leaves the amplifier through window 33.

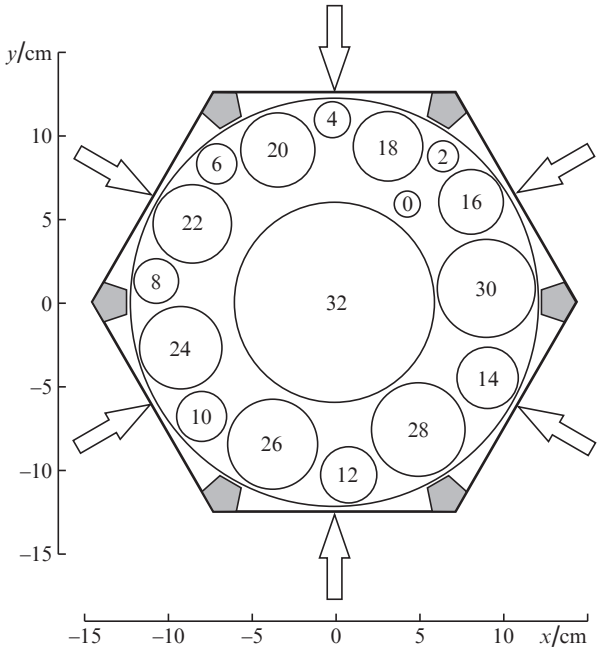

Figure 1. Schematic of the amplifier mirror unit. The numbers of the mirrors correspond to the number of beam transits across the amplifier prior to passing to the mirror. The output unit of the amplifier has the same set of mirrors with odd numbers. Arrows indicate the direction of VUV pump radiation. Dashed domains are opaque for pump radiation.

In modelling we calculated the gain for the conically expanding beam of laser radiation, whose divergence angle varied from $\Omega_1 = 0.95$ mrad (from the first to 31st transit) to $\Omega_2 = 22$ mrad (the 32nd and 33rd transits). The angles Ω_1 and Ω_2 are substantially larger than the angle of diffraction divergence; thus, diffraction was neglected in the model.

Kinetics of reactions in an N_2–XeF_2 mixture with VUV pumping has been studied in [6, 14, 15]. It was established that in the photolysis of XeF_2, excimer molecules XeF(B) and XeF(C) are generated in vibrationally excited states. Then, in VV- and VT-relaxation processes molecules transfer to zero vibration states of XeF(B_0,C_0). The rate of relaxation processes actually determines the pumping rate for upper laser levels of XeF(C_0).

The system of vibration levels for XeF(B,C) molecule comprises four effective levels: B and B_0 are vibrationally excited and unexcited levels of XeF(B), and C and C_0 are vibrationally excited and unexcited levels of XeF(C), respectively. The concentrations of these levels will be denoted by n_B, n_{B_0}, n_C, and n_{C_0}, respectively.

We consider pulses of duration $t_{pl} = 50$ ps (it is the FWHM value), which is substantially shorter than the characteristic time of vibrational relaxation for XeF(B,C). Hence, we may separately calculate the characteristics of the active medium and simulate the laser pulse amplification. A spatial distribution of the particle concentration in the amplifier was found by solving the system of integral-differential equations describing propagation of UV pump radiation and the balance equations for particle concentration in the active medium [8]:

$$\cos\Theta \frac{\partial I(r_w,\Theta,t_p)}{\partial r_w} = -\sigma_{VUV} I(r_w,\Theta,t_p) N_{XeF_2}, \quad (1)$$

$$\frac{\partial N_{XeF_2}}{\partial t_p} = -2\pi N_{XeF_2}\sigma_{VUV}\int_0^\pi I(r_w,\Theta,t_p)\sin\Theta\,d\Theta, \quad (2)$$

$$\frac{\partial n_B(x,y,t_p)}{\partial t_p} = \gamma_B N_f(x,y,t_p) - \tau_B^{-1} n_B(x,y,t_p) + k_{CB}^{N_2} n_C(x,y,t_p) M, \quad (3)$$

$$\frac{\partial n_C(x,y,t_p)}{\partial t_p} = \gamma_C N_f(x,y,t_p) - \tau_C^{-1} n_C(x,y,t_p) + k_{BC}^{N_2} n_B(x,y,t_p) M, \quad (4)$$

$$\frac{\partial n_{B_0}(x,y,t_p)}{\partial t_p} = \tau_{B_v}^{-1}[n_{B_0}^e(x,y,t_p) - n_B(x,y,t_p)] + k_{C_0B_0}^{N_2} n_{C_0}(x,y,t_p) M - \tau_{B_0}^{-1}(x,y,t_p), \quad (5)$$

$$\frac{\partial n_{C_0}(x,y,t_p)}{\partial t_p} = \tau_{C_v}^{-1}[n_{C_0}^e(x,y,t_p) - n_C(x,y,t_p)] + k_{B_0C_0}^{N_2} n_{B_0}(x,y,t_p) M - \tau_{B_0}^{-1} n_{C_0}(x,y,t_p), \quad (6)$$

$$\tau_{B_v}^{-1} = k_{B_v}^{N_2} M, \quad \tau_{C_v}^{-1} = k_{C_v}^{N_2} M. \quad (7)$$

Here, t_p is the time (pumping starts at $t_p = 0$); r_w is the distance from the lateral face of the laser chamber to the considered point of the active medium; x and y are the coordinates (distribution of the density of absorbed pump energy along amplifier axes z is assumed homogeneous); $I(r_w,\Theta,t_p)$ is the photon flux density of pump VUV radiation; Θ is the angle between the propagation direction of pump radiation and normal to the window surface; σ_{VUV} is the cross section of pump radiation absorption by XeF_2 molecules; N_{XeF_2} is the concentration of XeF_2 molecules; $N_f(x,y,t_p)$ is the number of acts of XeF_2 photolysis in unit volume per unit time at a point with the coordinates x, y, t_p; M is the concentration of buffer nitrogen molecules; γ_B and γ_C are quantum yields for XeF(B) and XeF(C) in the photolysis, respectively; $n_{B_0}^e$ and $n_{C_0}^e$ are the equilibrium concentrations of XeF(B_0) and XeF(C_0) molecules, respectively; $k_{B_v}^{N_2}$ and $k_{C_v}^{N_2}$ are the constants of vibrational relaxation of XeF(B) and XeF(C) in nitrogen medium; $k_{BC}^{N_2}$, $k_{B_0C_0}^{N_2}$, $k_{CB}^{N_2}$ and $k_{C_0B_0}^{N_2}$ are the constants of the exchange B ↔ C and B_0 ↔ C_0 in collisions with N_2 molecules; τ_B^{-1} =

$\tau_{BX}^{-1} + Q_B + k_{BC}^{N_2} n_B M$; $\tau_C^{-1} = \tau_{CA}^{-1} + Q_C + k_{CB}^{N_2} n_C M$; τ_{BX}^{-1} and τ_{CA}^{-1} are the probabilities of spontaneous emission on the corresponding transitions; $Q_B = \sum_i k_B^{(i)} R_i$ and $Q_C = \sum_i k_C^{(i)} R_i$ are the probabilities of quenching the states XeF(B) and XeF(C) by mixture components and products of photolysis with the concentrations R_i; and $k_B^{(i)}, k_C^{(i)}$ are the corresponding constants. A thorough analysis of kinetic processes in the active medium of amplifier versus mixture composition and values of constants used in the model is given in [11, 16–18].

Gain for the laser radiation beam is calculated in the cylindrical system of coordinates $r\varphi z_L$, where r and φ are the distances from the longitudinal beam axis and the azimuth angle, respectively; z_L is the distance covered by a 'head' part of the laser beam in the amplifier. The longitudinal axis of the laser beam coincides with the z_L axis, the position of the latter is determined by trajectory of laser beam motion in the amplifier. The initial point A($r = 0$, φ, $z_L = 0$) is at the centre of the input window 0 (Fig. 1). The maximal value of z_L, which is equal to the path length of the laser beam in the amplifier, is attained on the output mirror 33. The photon flux density of laser radiation $F(r,\varphi,z_L,t)$ and concentration $n_{C_0}(r,\varphi,z_L,t)$ were determined by solving the equations

$$\frac{\partial}{\partial t} n_{C_0}(r,\varphi,z_L,t) = -n_{C_0}(r,\varphi,z_L,t)\sigma_{C_0A}F(r,\varphi,z_L,t), \qquad (8)$$

$$\left[\frac{\partial}{\partial z_L} + K + \frac{1}{c}\frac{\partial}{\partial t} - n_{C_0}(r,\varphi,z_L,t)\sigma_{C_0A}\right]F(r,\varphi,z_L,t) = 0. \qquad (9)$$

Here and in what follows, $t = t_p - t_{pin}$ is the propagation time for the 'head' part of laser beam in the amplifier; t_{pin} is the time of introducing a laser beam into the amplifier, which is found from the condition of maximal amplification for input pulse and equals to 80 ns; $\sigma_{C_0A} = 9\times10^{-18}$ cm^2 is the cross-section of induced emission on the lasing transition C_0–A of XeF molecule [15]; $K = 2/(z_L + r_c)$ is the coefficient of laser radiation beam density reduction due to beam expansion [19]; r_c is the radius of curvature of laser radiation wavefront; and c is the speed of light.

Experiments and calculations were carried out for the mixture N_2 (380 Torr) and XeF_2 (0.2 Torr). The initial concentrations $n_C(x,y,0)$, $n_{C_0}(x,y,0)$, $n_B(x,y,0)$, and $n_{B_0}(x,y,0)$ were taken zero. Time dependence of photon flux density near input windows $I(0,\Theta,t_p)$ was chosen according to oscillograms of vacuum diode power and normalised to the total pumping energy E_{VUV} = 270 J, measured by a calorimeter inside the chamber. The leading edge duration of the pump pulse $I(r_w,\Theta,t_p)$ was 100 ns, and its zero-level duration was 330 ns.

The initial distribution $n_{C_0}(r,\varphi,0,0)$ was found by using two-dimensional interpolation methods issuing from the coordinates of point A(x, y, t_{pin}) at instant t_{pin} and the concentration $n_{C_0}(x,y,t_{pin})$ obtained by solving system of equations (1)–(7). When a beam propagates in the amplifier, the concentration $n_{C_0}(r,\varphi,z_L,t)$ in a domain of the head part of the beam is always equal to $n_{C_0}(r,\varphi,t)$ obtained issuing from the coordinates A($x,y,t + t_p$) and concentration $n_{C_0}(x,y,t + t_p)$. Concentration $n_{C_0}(r,\varphi,z_L,t)$ in other points of the laser beam was calculated from system of equations (8), (9).

At the amplifier input, the flux density distribution $F(r,\varphi,z_L,t)$ in the beam was described by the Gaussian profile:

$$F_{in}(r,\varphi,t) = F_{max}\exp\left(-2\frac{r^n}{R_{st}^n}\right)\exp\left[-\frac{(t-t_{max})^2}{t_{pl}^2}4\ln 2\right], \qquad (10)$$

where t_{max} is the time needed to reach the maximal flux density F_{max}; t_{pl} is the input pulse duration; and R_{st} is the radius of the input laser beam with respect to the intensity level 1/e^2. The index of power n was taken two for Gaussian and four for super-Gaussian radial distributions of the flux density F_{in}. The range of r variation was determined by the radius R_0 of the input window (from zero to the beam radius $R_b = R_0$). In beam propagation across the amplifier, the radius R_b varied from 0.5 cm on the input window to 6.0 cm on the output window. The flux density on a lateral side of the beam $r = R_b$ is calculated by formula (10). Distribution over φ was assumed uniform, and F_{max} was found from the condition of the normalising energy to the input beam energy E_{in}.

The power of amplified spontaneous emission in this system did not exceed 200 W [8], which is substantially lower than the laser radiation power in the amplifier; hence, it was neglected in calculations. Balance equations for the particle concentration in the active volume of the amplifier were solved by the Gear method. The wave equation was solved by the Runge–Kutta method with a constant step. The step value in calculations was 5×10^{-13} s. The maximal inaccuracy in these calculations was at most 10%.

The model was tested with various gaseous mixtures prior to system modernisation [10, 20] and after it [21] (at E_{VUV} = 260 J). In all the works, a good agreement was observed between experimental data and results of modelling [10, 20, 21].

4. Results and discussion

The calculated distribution of specific absorbed pump energy E_{abs} in the transverse cross section of the amplifier is shown in Fig. 2. It reaches the maximal value (7.5 mJ cm^{-3}) on the surface of windows for input pump radiation ($r_w = 0$). On the longitudinal axis of the amplifier E_{abs} falls to 0.5 mJ cm^{-3}. Due to partial screening of pump radiation, E_{abs} reduced to 4 mJ cm^{-3} near opaque regions. From the total energy of pump VUV radiation E_{VUV} = 270 J, the energy of E_{abs} = 182.5 J is absorbed in the laser chamber. The rest energy is absorbed on webbings (shaded domains in Fig. 1) and leaves the chamber through input windows.

Nonuniform distribution of absorbed pump energy results in nonuniform distribution of the small-signal gain $g(r,\varphi)$ in the transverse cross section of the laser beam. In [22], this

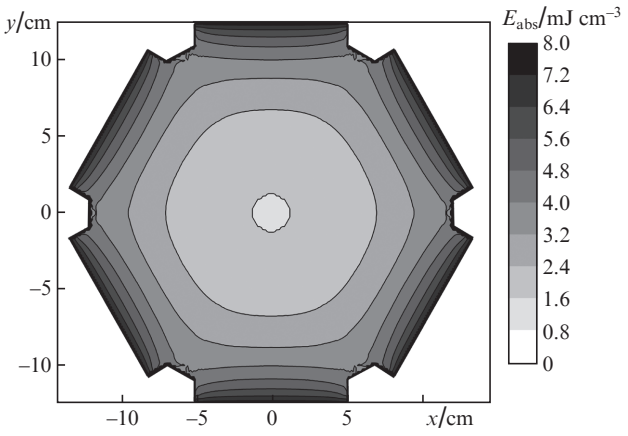

Figure 2. Calculated distribution of specific absorbed pump energy E_{abs} in the transverse cross section of the amplifier. The total pump energy is E_{VUV} = 270 J.

problem was studied by numerical simulation. A laser beam with uniform distribution of energy density in the transverse cross section $W_{in} = 0.05\times10^{-6}$ J cm^{-2} (with $t_{p\,in} = 80$ ns) passed to the amplifier input. At the output from the amplifier, the energy density of laser radiation W_{out} near the external boundary of the beam ($r = R_b$) was 52×10^{-6} J cm^{-2} (see Fig. 2 in [22], where $g = W_{out}/W_{in} \approx 1000$). At the axis of the laser beam ($r = 0$), the energy density reduced to 15×10^{-6} J cm^{-2} ($g \approx 300$). Thus, it was shown in [22] that in the regime of a small-signal gain, the parts of the laser beam adjacent to its external boundary are amplified by approximately three times than at the axis.

In the present work, the influence of the energy E_{in} and of the input beam spatial density distribution $W_{in}(r)$ on the energy E_{out} and on the energy spatial distribution $W_{out}(r,\varphi,t)$ of the amplified beam is studied. The input beam energy varied in the range 0.1–6 mJ. At a higher input beam energy, the energy of the output beam E_{out} did not change. The radius of the input beam R_{st} at the intensity level of $1/e^2$ varied from 0.5 to 0.22 cm. Amplification of the input beam with a super-Gaussian radial intensity distribution was also studied. In this case, the radius R_{st} was taken 0.5 cm and the index of power n was equal to four.

Radial distributions of the energy density W_{in} of the input beam having the energy $E_{in} = 2$ mJ are shown in Fig. 3 for various values of R_{st}. The maximal energy density at the beam axis $W_{in}(0) \approx 25$ mJ cm^{-2} is attained at the minimal radius of the input beam $R_{st} = 0.22$ cm. In this case $W_{in}(R_{st}) = 3.4$ mJ cm^{-2}. At the input beam radius increased to 0.5 cm, the distribution $W_{in}(r)$ becomes more uniform: $W_{in}(0) = 5.7$ mJ cm^{-2} and $W_{in}(R_{st}) = 0.78$ mJ cm^{-2}. In the case of a super-Gaussian distribution [curve (*1*)] $W_{in}(0)$ and $W_{in}(R_{st})$ are 4.15 and 0.56 mJ cm^{-2}, respectively. In experiments, the distribution $W_{in}(r)$ [curve (*2*)] is close to that calculated for $R_{st} = 0.5$ cm.

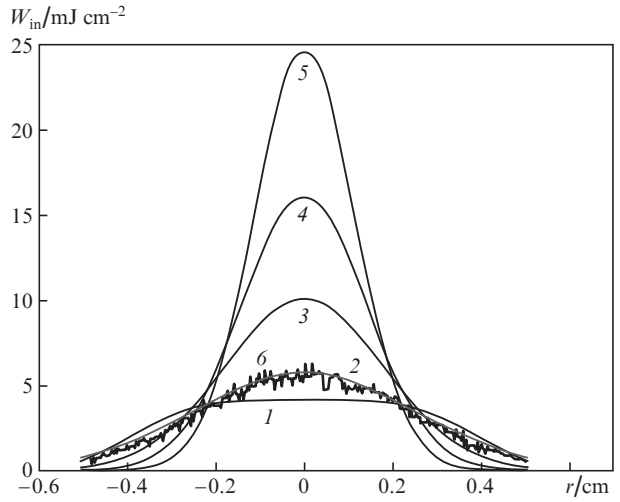

Figure 3. (*1*) Super-Gaussian and (*2–5*) Gaussian radial distributions of the input radiation energy density $W_{in}(r)$ at R_{st} = (*1*, *2*) 0.5, (*3*) 0.35, (*4*) 0.28 and (*5*) 0.22 cm. Curve (*6*) is experimental. The energy of input laser radiation is $E_{in} = 2$ mJ.

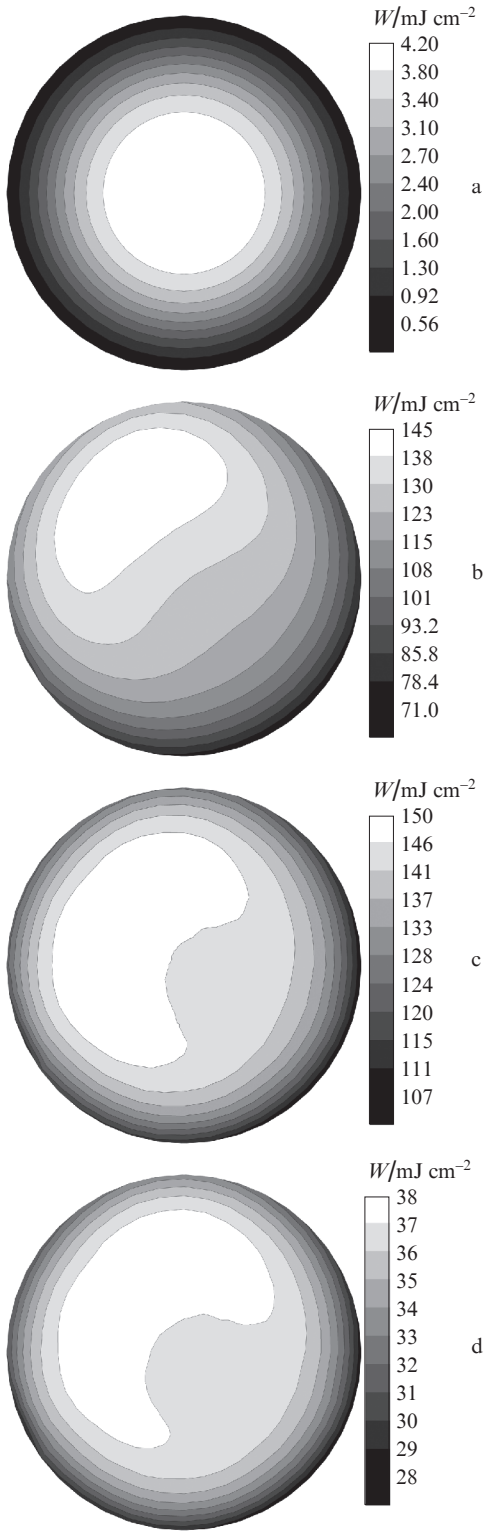

Figure 4. Energy density distributions of laser radiation W in various cross sections of the beam: (a) in the input beam (super-Gaussian distribution), (b) on 25th mirror, (c) on 31st mirror and (d) on the output window.

In passing through the amplifier, the energy density distribution in the transverse cross section of the laser beam $W(r,\varphi,t)$ instantaneously varies. Dynamics of $W(r,\varphi,t)$ in the case of a super-Gaussian distribution is shown in Fig. 4. The energy density $W_{in}(0,\varphi,0)$ at the input beam axis is ~4 mJ cm^{-2}. In 15 transits across the amplifier, $W(0,\varphi,t)$ reaches 52 mJ cm^{-2} and the distribution becomes nonuniform.

On mirror 25, the maximal energy density of laser radiation at the beam axis $W(0,\varphi,t)$ is 145 mJ cm^{-2} (Fig. 4b). In this domain, the laser radiation destroys up to 96% of $XeF(C_0)$

molecules. Then, $W(0,\varphi,t)$ changes negligibly and remains equal to ~150 mJ cm^{-2}, whereas the laser beam energy rises due to increasing $W(R_b)$ on its boundary. Near the 31st mirror, $W(R_b)$ reaches ~110 mJ cm^{-2} (Fig. 4c) and the spatial distribution $W(r,\varphi,t)$ weakly depends on the azimuthal angle (within ~2%). An increase in the laser beam radius R_b to 5.5 cm on the output mirror results in a reduction of $W(0)$ and $W(R_b)$ to 36 and 32 mJ cm^{-2}, respectively (Fig. 4d).

Hence, at E_{in} = 2 mJ, the calculated energy density of the laser beam weakly depends on the azimuthal angle, which still holds true at higher input energies. Thus, in what follows we will consider only radial distributions $W(r,0,t)$ which we will denote as $W(r,t)$.

Figure 5 shows the dependences of the laser radiation energy E_{out} at the amplifier output on the input beam energy calculated for various R_{st}. Curve (*1*) corresponds to a super-Gaussian intensity distribution. An increase in R_{st} leads to a higher energy density at the beam periphery $W_{in}(R_b)$ (Fig. 3) and increases the output laser radiation energy in the whole range of E_{in} variation. The maximal energy reaches 4.1 J at an input energy of 6 mJ. Calculations show that if E_{in} increases from 0.1 to 1.5 mJ, the output energy E_{out} rapidly increases due to growth of $W(0)$ and $W(R_b)$. At E_{in} = 1 mJ, the value of $W(0)$ near mirror 31 reaches 170–188 mJ cm^{-2} at R_{st} = 0.5–0.22 cm and under further increase in the input beam energy changes negligibly (to 190 mJ cm^{-2} at E_{in} = 6 mJ). If E_{in} > 1 mJ, at all values of R_{st} the increase in the laser radiation energy at the amplifier output the occurs due to increasing $W(r \approx R_b)$.

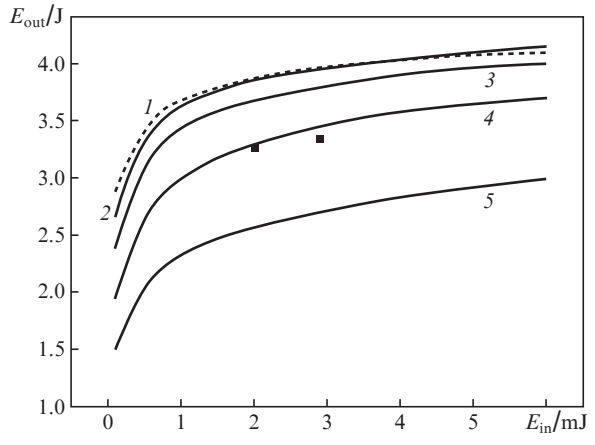

Figure 5. Dependences of the laser energy at the output from the XeF(C–A) amplifier vs. input beam energy, corresponding to (*1*) super-Gaussian and (*2–5*) Gaussian intensity distributions at R_{st} = (*1*, *2*) 0.5, (*3*) 0.35, (*4*) 0.28 and (*5*) 0.22 cm. Points refer to experimental data.

Numerical simulations performed previously [10, 11] have shown that the energy of 3 J and more can be reached on this installation. The laser radiation energy obtained experimentally at the pulse duration of 2 ps was E_{out} = 2 J. A further increase in E_{in} leads to small-scale self-focusing and prevents an increase in the output energy of laser radiation. Increasing the duration of the radiation pulse entering the XeF(C–A) amplifier to 50 ps gives a possibility to reduce the maximal radiation intensity to 12 GW cm^{-2}. In this case, optimisation of experimental conditions (the input pulse energy, input beam profile, instant of beam injection into the amplifier, pressure of XeF_2 and N_2 vapours, divergence angle for amplified radiation) allows one to reach the amplifier output energy of 3.21 J. When the input energy varied from 2 to 3 mJ, the output energy, contrary to the calculation results, was actually constant (points in Fig. 5). Thus, gain was saturated with respect to input energy.

The values of E_{out} calculated at R_{st} = 0.5 cm, E_{in} = 2 and 3 mJ are 3.88 and 3.98 mJ, respectively, which is higher than experimental values. The radial distribution of the energy density $W_{out}(r)$ at the output from the amplifier calculated for R_{st} = 0.5 cm substantially differs from experimental. Calculated and experimental radial distributions $W_{out}(r)$ normalised to unity are shown in Fig. 6. One can see that as the input beam radius R_{st} increases, which results in a greater $W_{in}(0)$ (see Fig. 3), $W_{out}(R_b)$ also increases. Difference in distributions $W_{out}(r)$ for Gaussian and super-Gaussian beams is not substantial. This is explained by the fact that, according to our calculations, in the integral over the entire active volume the pump energy absorbed at the centre of the amplified beam is smaller than at the periphery. The Gaussian intensity distribution of the input beam (a higher energy density at the axis) compensates for a smaller gain at the central part.

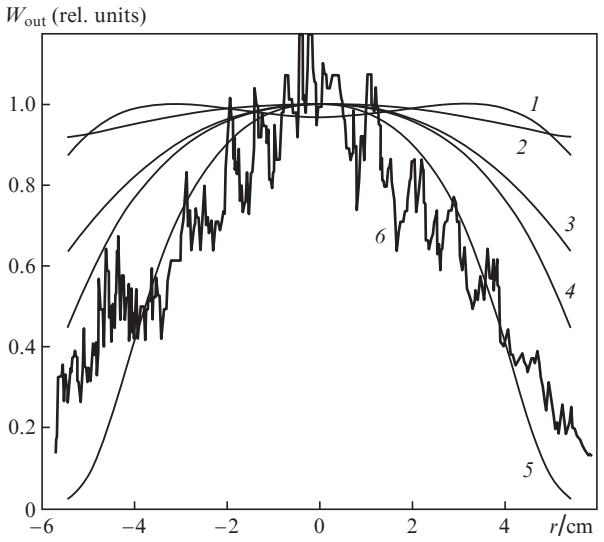

Figure 6. (*1*) Super-Gaussian and (*2–5*) Gaussian energy density radial distributions of laser radiation in the output window at R_{st} = (*1*, *2*) 0.5, (*3*) 0.35, (*4*) 0.28 and (*5*) 0.22 cm. Curve (*6*) refers to experimental data. The energy of input beam is E_{in} = 2 mJ.

In order to demonstrate dynamics of the ratio of laser energy densities at the external boundary $[W_{out}(R_b)]$ and at the beam axis $[W_{out}(0)]$ consider the relative difference

$$\Delta = [W(0) - W(R_b)]/[W(0) + W(R_b)]. \quad (11)$$

Dependences of Δ on the number N of pulse transits across the amplifier for various input beam radii R_{st} are presented in Fig. 7. The greater the R_{st}, the lower the N at which Δ starts to reduce; this means that $W(R_b)$ increases more rapidly as compared to $W(0)$. At a super-Gaussian intensity distribution of the input beam, Δ reduces from ~0.6 at the amplifier input to 0.07 at the amplifier output. However, at R_{st} = 0.22, the value of Δ changes negligibly. In experiments on laser beam amplification, the energy density $W(R_b)$ increased substantially less than in the calculations with R_{st} =

0.5 cm. Dynamics of the experimental relative difference Δ is shown by the dashed line in Fig. 7. On the input amplifier window, the radial distribution $W_{in}(r)$ corresponds to the Gaussian distribution at $R_{st} = 0.5$ cm (see Fig. 3). In the result of amplification, the value of Δ changes from 0.65 at the amplifier input to 0.6 at its output.

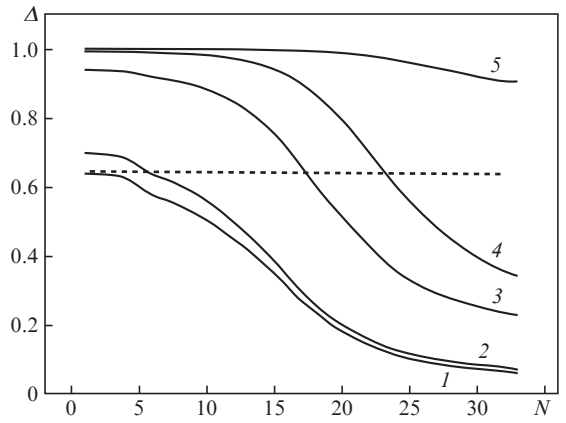

Figure 7. Dependences of relative difference Δ on the number N of laser pulse transits across the amplifier, corresponding to (*1*) super-Gaussian and (*2–5*) Gaussian intensity distributions at R_{st} = (*1*, *2*) 0.5, (*3*) 0.35, (*4*) 0.28 and (*5*) 0.22 cm. Dashed line refers to experimental data.

To understand reasons for this experimental discrepancy, we detected the spatial energy density distributions for radiation passed through a 'cold' (without pumping) amplifier and for the same radiation passed through air along a distance of 41.7 m equal to the amplifier length. In both the cases, a tooth diaphragm was used for limiting the initial radiation. Radial energy density distributions of laser radiation normalised to unity are shown in Fig. 8. One can see that the system of mirrors in the amplifier noticeably changes the beam profile: its diameter at the level of $1/e^2$ reduces almost twice. We relate

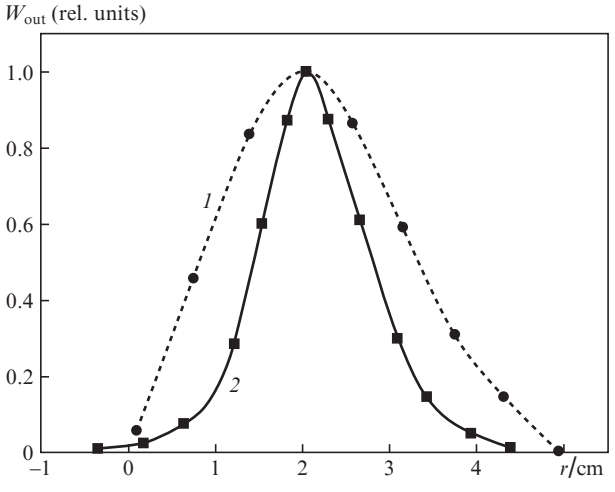

Figure 8. Measured radial energy density distributions of the laser beam W_{out} (*1*) while transporting it through air along a distance of 41.7 m and (*2*) after it has passed through the amplifier (cold). The radiation wavelength is λ = 475 nm, and the pulse duration is 50 ps.

this phenomenon with imperfect flatness of mirrors. In calculations, such a reduction of the diameter at the amplifier output is equivalent to a reduction of the diameter of the beam entering the amplifier. In this case, as it follows from Fig. 5, the energy of amplified radiation noticeably falls.

In experiments we varied the intensity distribution at the amplifier output by increasing the input beam divergence using for this purpose a telescope with magnification 3×. However, this resulted in higher energy losses of the radiation passed through the cold amplifier. Amplification of such a beam is not accompanied with an increase in the output radiation energy. On the other hand, reduction of the divergence lowered the energy of amplified radiation.

5. Conclusions

Thus, we present the results of experimental and numerical investigations of spatial and energy characteristics of XeF(C–A) amplifier radiation versus the energy and spatial distribution of the energy density of input laser radiation. The energy of laser radiation obtained experimentally at a 50-ps pulse duration was 3.2 J. It is shown that this value is close to the saturation energy of the amplifier. In calculations, the maximal output energy is 4.1 J and corresponds to actually total saturation energy of the amplifier. Discrepancy between theoretical and experimental results is explained by the imperfect mirror quality in the optical scheme of the amplifier. After removing this drawback and compressing the amplified pulse to the initial duration of 50 ps, the output power of laser system THL-100 will reach ~82 TW.

Acknowledgements. This work was supported by the Russian Foundation for Basic Research (Grant No. 16-08-00204), and the experimental study was supported by the Russian Science Foundation (Grant No. 15-19-10021).

References

1. Basov N.G., Zuev V.S., Mikheev L.D., Stavrovskii D.B., Yalovoi V.I. *Kvantovaya Electron.*, **4** (11), 2453 (1977) [*Sov. J. Quant. Electron.*, **7** (11), 1402 (1977)].
2. Bischel W.K., Nakano Y.Y., Eckstrom D.J., Hill R.M., Huestis D.L., Lorents D.C. *Appl. Phys. Lett.*, **34**, 565 (1979).
3. Mikheev L.D. *Laser Part. Beams*, **10**, 473 (1992).
4. Basov N.G., Zuev V.S., Kanaev A.V., Mikheev L.D., Stavrovskii D.B. *Kvantovaya Electron.*, **6**, 1074 (1979) [*Sov. J. Quant. Electron.*, **5**, 629 (1979)].
5. Tcheremiskine V.I., Sentis M.L., Mikheev L.D. *Appl. Phys. Lett.*, **81**, 403 (2002).
6. Malinovskii G.Ya., Mamaev S.B., Mikheev L.D., Moskalev T.Yu., Sentis M.L., Cheremiskin V.I., Yalovoi V.I. *Kvantovaya Elektron.*, **31**, 617 (2001) [*Quantum Electron.*, **31**, 617 (2001)].
7. Tcheremiskine V., Uteza O., Mislavskii V., Sentis M., Mikheev L. *Proc. SPIE Int. Soc. Opt. Eng.*, **6346**, 634613 (2007).
8. Alekseev S.V., Aristov A.I., Grudtsyn Ya.V., Ivanov N.G., Koval'chuk B.M., Losev V.F., Mamaev S.B., Mesyats G.A., Mikheev L.D., Panchenko Yu.N., Polivin A.V., Stepanov S.G., Ratakhin N.A., Yalovoi V.I., Yastremskii A.G. *Kvantovaya Elektron.*, **43**, 190 (2013) [*Quantum Electron.*, **43**, 190 (2013)].
9. Alekseev S.V., Aristov A.I., Ivanov N.G., Kovalchuk B.M., Losev V.F., Mesyats G.A., Mikheev L.D., Panchenko Yu.N., Ratakhin N.A. *Laser Part. Beams*, **31**, 17 (2013).
10. Alekseev S.V., Ivanov N.G., Losev V.F., Panchenko Yu.N., Yastremskii A.G. *Opt. Atmos. Okeana*, **26**, 863 (2013).
11. Ivanov N.G., Losev V.F., Panchenko Yu.N., Yastremskii A.G. *Opt. Atmos. Okeana*, **27**, 326 (2014).
12. Yastremskii A.G., Ivanov M.V., Ivanov N.G., Losev V.F. *Opt. Atmos. Okeana*, **29**, 121 (2016).

13. Losev V.F., Alekseev S.V., Ivanov M.V., Ivanov N.G., Mesyats G.A., Mikheev L.D., Panchenko Yu.N., Ratakhin N.A., Yastremsky A.G. *Book of Abstracts of the 21st Int. Symp. on High Power Laser System and Applications* (Gmunden, Austria, 2016) p. 25.
14. Tcheremiskine V.I. *Ph.D. Thesis*; http://http://www.lp3.univ-mrs.fr/.
15. Bishel W.K., Eckstrom D.J., Walker H.C., Tilton R.A. *J. Appl. Phys.*, **52**, 4429 (1981).
16. Mikheev L.D., Stavrovskii D.B., Zuev V.S. *J. Russ. Laser Res.*, **16**, 427 (1995).
17. Brashers H.C., Setser D.W. *J. Chem. Phys.*, **76**, 4932 (1982).
18. Black G., Sharpless R.L., Lorents D.C., Huestis D.L., Gutcheck R.A., et al. *J. Chem. Phys*., **75**, 4840 (1981).
19. Kuznetsova T.I., Mikheev L.D. *Kvantovaya Electron*., **38**, 969 (2008) [*Quantum Electron.*, **38**, 969 (2008)].
20. Losev V., Alekseev S., Ivanov N., Kovalchuk B., Mikheev L., Mesyats G., Panchenko Yu., Puchikin A., Ratakhin N., Yastremsky A. *Proc. SPIE Int. Soc. Opt. Eng*., **7993**, 799317 (2011).
21. Yastremskii A.G., Ivanov N.G., Losev V.F., Panchenko Yu.N. *Proc. SPIE Int. Soc. Opt. Eng*., **9255**, 925528 (2015).
22. Ivanov N.G., Ivanov M.V., Losev V.F., Yastremskii A.G. *Izv. Vyssh. Uchebn. Zaved., Ser. Fiz*., **59**, 65 (2016).